

Fluorescence study of Bovine Serum Albumin and Ti and Sn Oxide Nanoparticles Interactions.

Denisio M. Togashi,^{a,b} Alan G. Ryder,^{a,b} Deirdre Mc Mahon,^a Peter Dunne,^b and James McManus.^b

^a Nanoscale Biophotonics Laboratory, National Centre for Biomedical Engineering Science, National University of Ireland, Galway, Galway, Ireland.

^b Chemistry Department, National University of Ireland, Galway, Galway, Ireland.

ABSTRACT

Nanochemistry offers stimulating opportunities for a wide variety of applications in the biosciences. Understanding of the interaction of nanoparticles with biomolecules such as proteins is very important as it can help better design and fabricate nanocomposites for applications in diagnostics, drug delivery, and cell monitoring. In this work, the interaction of Bovine Serum Albumin (BSA) and two types of metal oxide nanoparticles (titanium and tin) have been studied using the intrinsic fluorescence of tryptophan residue from the proteins measured by steady state and time resolved fluorescence techniques. The nanoparticles which were fabricated using a novel synthetic process have average sizes of ~2 nm (SnO₂) and ~6 nm (estimated for TiO₂) and have very high solubilities in a variety of solvents. The Stern-Volmer plots indicate an effective quenching process by TiO₂ nanoparticles whereas SnO₂ nanoparticles have a lower quenching efficiency for BSA fluorescence. Static quenching is the major contribution in the overall process which may indicate a high degree of association between protein and nanoparticles. The difference in BSA fluorescence quenching efficiency between the two types of nanoparticles can be explained by the non-covalent interaction differences and the thermal stability of protein-nanoparticle associated species for both materials.

Keywords: Fluorescence, nanoparticles, bovine serum albumin, protein, TiO₂, SnO₂.

1. INTRODUCTION

Nanoparticles (NP) have many diverse applications in the life and physical sciences¹. The small size and the large surface areas confer very specific chemical, physical, and spectroscopic features. Metal nanoparticles are widely used for a variety of applications like Surface Enhanced Raman Spectroscopy (SERS), while semiconductors (quantum dots) are used for biomedical imaging. Metal oxide NPs are another class in which chemical properties can be manipulated, and their surface properties can be tailored by introduction of ligand functionality to provide versatility with regard to target specificity¹. NP-based probes have been used as labels in biological systems, with great potential for bioimaging, diagnostic and therapeutic purposes. Understanding the interactions of NP with biological molecules is important for the sensor applications.

It is well documented that protein adsorption is the first process which occurs upon implantation of a biomaterial into a biological system. Protein molecules adsorbed onto the interface between a biomaterial and the physiological environment can greatly influence and control subsequent reactions and even determine acceptance or rejection of an implant material². Hence, cells do not contact the biomaterial directly, but interact with the adsorbed protein layer. Control of the protein structure on adsorption, with regard to properties such as orientation, conformation, and packing arrangement, is imperative in relation to the number of bioactive sites and cellular response³. In situations where protein adsorption is desirable to reduce immunogenicity and induce cellular integration, retention of the native protein structure and function is of paramount importance. The function and form of proteins is dependant on their tertiary structure which is determined by the precise way in which the protein chains fold about each other. This tertiary structure can be influenced by the surrounding environment, and this can dramatically influence the effect of the protein on the host organism. Proteins which have become misfolded, and changed their tertiary structure through chemical or physical distortion can have adverse effects on the organisms metabolism, particularly at the cellular level⁴.

Serum albumin is the most abundant protein in mammalian plasma, with a well-known structure. BSA is an ideal protein for intrinsic fluorescence measurement due to the presence of two intrinsic tryptophan (Trp) residues. It is also the main protein contributing to the colloid osmotic pressure of the blood⁵. In crystal form, the serum albumin molecule

is postulated to be heart-shaped or triangular, with dimensions of $8.0 \times 8.0 \times 4.0$ nm. However, in solution, it is assumed to be ellipsoid in shape, with a predicted size of $\sim 3.8 \times 15$ nm. BSA is a single polypeptide chain (583 amino acids) with a molecular mass of 66.4 kDa. The serum albumin molecule is built from three structurally homologous domains: I, II, and III. There is a net charge gradient along the molecule, with decreasing net negative charge from domain I to domain III. At physiological pH, the net charges for domains I, II and III are -9 , -8 , and -2 , and -11 , -7 , and $+1$ for human and bovine serum albumin, respectively. The isoionic point of albumins, i.e. the pH of a thoroughly deionised solution, is ~ 5.2 ⁵. Hence, in neutral solution, the molecule is, as a whole, negatively charged.

The intrinsic fluorescence of albumin molecules is largely attributed to Tryptophan (Trp) residues, with only a minor contribution by the numerous tyrosines depending on the excitation wavelength selected. Trp is highly sensitive to its local environment, and can be used to observe changes in the fluorescence emission spectra due to protein conformational changes, binding to substrates, and denaturation.⁶

The main objective of this work was to assess the intrinsic Trp fluorescence of BSA in the presence of TiO_2 and SnO_2 NPs in solution. With regard to the protein and NPs in solution, the type of quenching observed implies that a complex is formed between the NPs and BSA, and this effect was much stronger for TiO_2 NPs than for SnO_2 NPs. Up to the present time, these NPs had not been tested with regard to protein interactions; the work carried out in this study was quite exploratory. The results are discussed below with regard to potential reasons behind the observations of the present study, with related findings and possible explanations from the literature to date.

2. MATERIALS AND METHODS

2.1 Materials:

Bovine serum albumin (BSA) of purity 99+ % (catalogue no. A7638) and N-acetyl-DL-tryptophan (NAT) were purchased from Sigma-Aldrich. All reagents were used without further purification. Phosphate buffered saline tablets for 0.01 M phosphate buffer (PBS), 0.0027 M potassium chloride, and 0.137 M sodium chloride at pH 7.4 were purchased from Aldrich. All solutions were made up with purified water from a Milli-Q Millipore system. The soluble metal oxide nanoparticles were synthesised in-house using a proprietary method developed at NUI, Galway.⁷

2.2 Sample preparation:

Stock solutions of 10^{-3} M serum from bovine albumin in PBS were prepared and recalibrated by measuring the absorbance at 280 nm ($\epsilon = 43,600 \text{ M}^{-1} \text{ cm}^{-1}$). Stock solutions of TiO_2 (0.4g/l) and SnO_2 (4.13 g/l) in deionised water were prepared from which further dilutions were made for experimental purposes prior to measurement. On dissolution of the TiO_2 nanocrystalline powder in PBS buffer, flocculation occurred, presumably due to the salt concentration. Other buffers, such as HEPES and Tris-buffered saline, were then prepared to determine suitable alternatives for use in solution-based experiments; however, all displayed cloudiness and flocculation with TiO_2 in solution. A 1:100 dilution of PBS in water was also prepared which appeared clear upon addition of TiO_2 nanocrystalline powder; however, its buffering ability appeared to be lost at this dilution as determined by testing with a pH meter and dropwise addition of acid (1 M HCl) and base (1 M NaOH) solutions. For this reason, deionised water was used in all solution-based experiments utilizing TiO_2 . In general, the samples were prepared and used at same day. In the experiments where a mixture of BSA and nanoparticles were required, the concentrations of protein were 2.5×10^{-6} M, while in a mixture of NP and tryptophan compound concentration was around 10^{-5} M. The prepared solutions were allowed to equilibrate for a time period of 30 min to 1 hour prior to measurement.

2.3 Absorption measurements:

Absorbance measurements were made using a Shimadzu UV-1601 UV-Visible spectrophotometer (Shimadzu, Kyoto, Japan). Unless otherwise stated, a wavelength range of 200–500 nm was used and absorbance was measured in 0.5 nm steps. For solution measurements, baseline was always set and measured using the relevant blank (i.e. PBS or water) in both the reference and sample cuvettes prior to absorbance measurements of samples. The final spectrum is an average of three independent measurements.

2.4 Steady-state fluorescence measurements:

Fluorescence emission measurements were made using a Cary Eclipse Fluorescence Spectrophotometer (Varian, Mulgrave, Victoria, Australia). Unless otherwise stated, the following settings were generally used: λ_{EX} , 295 nm; scan range, 305–450 nm; scan rate, 600 nm/min; excitation and emission slits, 5 nm; data interval, 1 nm. Alternative measurement settings are indicated in the relevant experimental procedures. The inner filter effect was minimised by ensuring that the sample absorbance at the excitation wavelength was less than 0.1 in a square quartz cuvette or by using a triangular cuvette (for high absorption samples) in fluorescence measurements. In the case of square cuvette the filter inner effect was also reduced by correcting the fluorescence intensity using the follow expression⁶:

$$I_{f(corr)} = I_{f(meas)} \times \text{antilog}[(OD_{ex} + OD_{em})/2] \quad (1)$$

Where, OD_{ex} and OD_{em} are the optical density of excitation wavelength and emission wavelength. In this work, we assumed that the emission optical density is very low by comparison to the excitation wavelength. All the fluorescence spectra were corrected using a blank solution. The final spectrum is an average of three independent measurements where the intensity is also corrected by the optical density value at the excitation.

2.5 Fluorescence lifetime measurements:

Fluorescence lifetime measurements were made using a FluoTime 200 Fluorescence Lifetime Spectrometer (PicoQuant), using time correlated single photon counting (TCSPC). The protein solutions were excited using Light Emitting Diode with centre wavelength of 295 nm, which was pulsed at 20 MHz using a PDL-800B laser/LED driver (PicoQuant, Germany). Ludox solution (Aldrich) was used to generate an instrument response function (IRF) prior to measurement of sample lifetimes. The measured count rate (proportional to the intensity of the sample) was monitored during data collection to ensure that they remained less than 1% of the pulse rate to prevent pulse pile-up effects to maintain Poisson statistics. All measurements were stopped at a count of 10,000 in the time channel of maximum intensity. Results were analysed using the FluoFit, Version 3.2.0 (PicoQuant) software package, which implements multi-exponential fluorescence decay fitting using nonlinear least-squares error minimization analysis. The goodness of the fit was assessed by the chi-squared value of less than 1.2 and a residual trace that was symmetric about the zero axes. The final result is an average of three independent measurements.

3. RESULTS AND DISCUSSION

3.1 TEM of nanoparticles:

Metal oxide NPs can be prepared by a number of different methods, including the sol–gel method (which involves arrested precipitation), chemical vapour deposition and physical vapour deposition. In this work soluble TiO_2 and SnO_2 NPs were prepared in the Chemistry Department, NUIG using a patented aqueous based method.⁷ These nanoparticles are fully characterized and the size determined by X-ray powder diffractometry and transmittance electron microscopy. In Fig. 1, SnO_2 clusters with an average size of less than 10 nm can be observed at a magnification of 200K. An accurate determination of size by X-ray powder diffractometry shows that the individual SnO_2 nanoparticles are ~ 1.9 nm in size. The TiO_2 nanoparticles have multiple crystalline phases (at room temperature) which cause inaccuracy in size determination. After annealing at high temperature, a particle size ~ 6 nm was estimated. For the purpose of this work, we assumed the same size at room temperature. In the calculation for Molar concentration, oxide metal densities of 6.95 g/cm³ and 3.89 g/cm³ are assumed for SnO_2 and TiO_2 nanoparticles, respectively.⁸

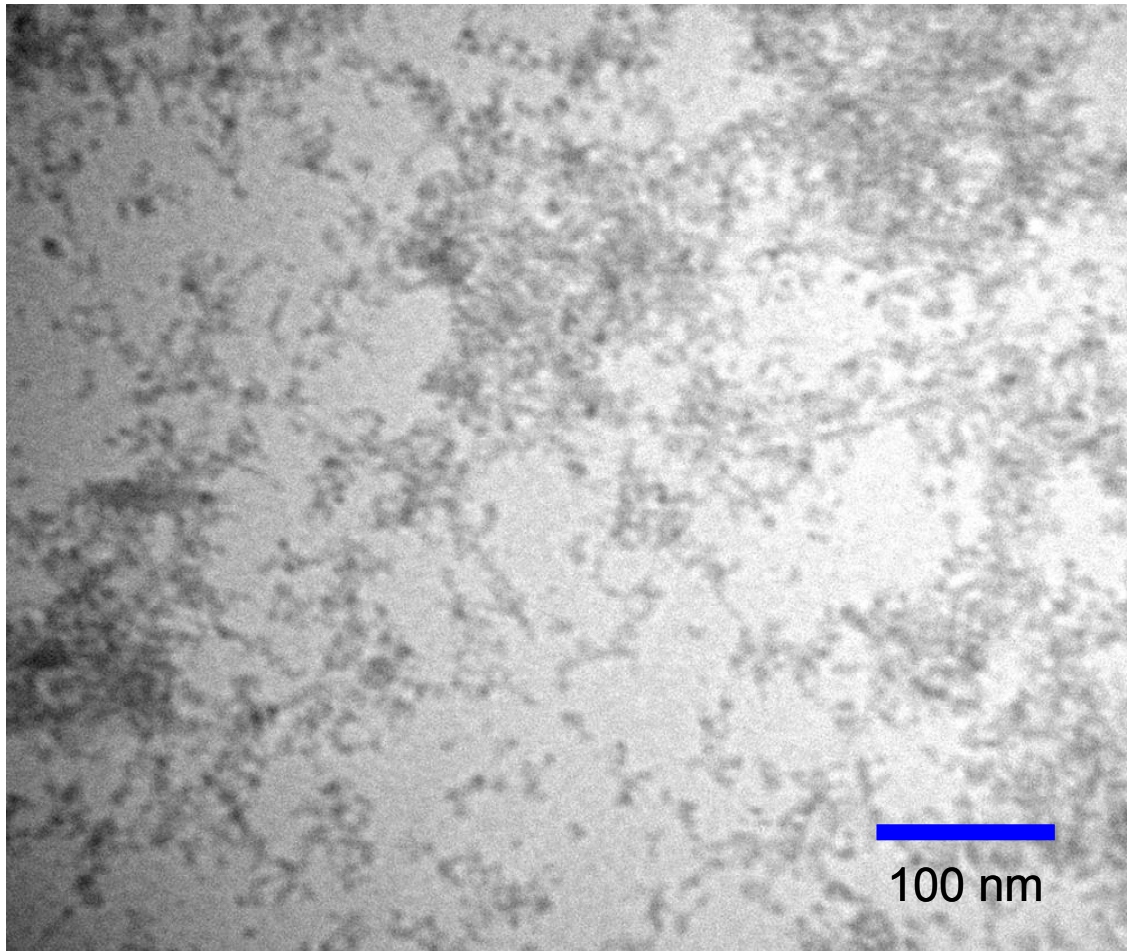


Fig. 1. Transmission Electron Microscopy images of SnO₂ nanoparticles magnified 200k times.

3.2 UV Absorption and Fluorescence Spectra of Nanoparticles and Nanoparticles/BSA:

Steady state absorption measurements were made for aqueous solutions of SnO₂ NP and TiO₂ NP in the presence of BSA (Fig. 2). It is clear that the NP absorption edge occurs very close to the Tryptophan (Trp) absorption band of BSA. The wavelength edge is around 270 nm for SnO₂ NP and around 280 nm for TiO₂ NP, while the protein band absorption maximum is also around 280 nm (Fig. 2C). The interaction between BSA and NP was verified by subtracting the NP UV absorption spectrum from the BSA/NP mixture UV absorption spectra at the same nanoparticles concentration. The BSA absorption band calculated from the mathematical subtraction in BSA/NP mixture did not show any changes with different NP concentration, that is, no red or blue shift was observed. On the other hand, the nanoparticle concentration effect on the overall spectra in presence of protein can be better observed if the protein UV spectrum is subtracted from BSA/NP mixture UV spectra, and compared with the absorption spectra of nanoparticle in absence of BSA, as shown in figure 2D. If no interaction occurs, it would be expected that the calculated absorption spectrum of BSA/NP mixture (BSA/NP spectrum minus BSA spectrum) be similar to NP absorption spectrum, at the same NP concentration. The UV spectrum of 100 mg/l SnO₂ NP is observed not to be perturbed by the presence of BSA. However, the presence of BSA protein produces an increase in the optical density at long wavelengths for 50 mg/l TiO₂ NP solution. This may indicate that the protein is inducing an increase in TiO₂ NP size probably by cluster formation (aggregation) which leads to increased light scattering. In the absence of protein, the nanoparticle absorption is linear with the concentration in the range studied.⁹

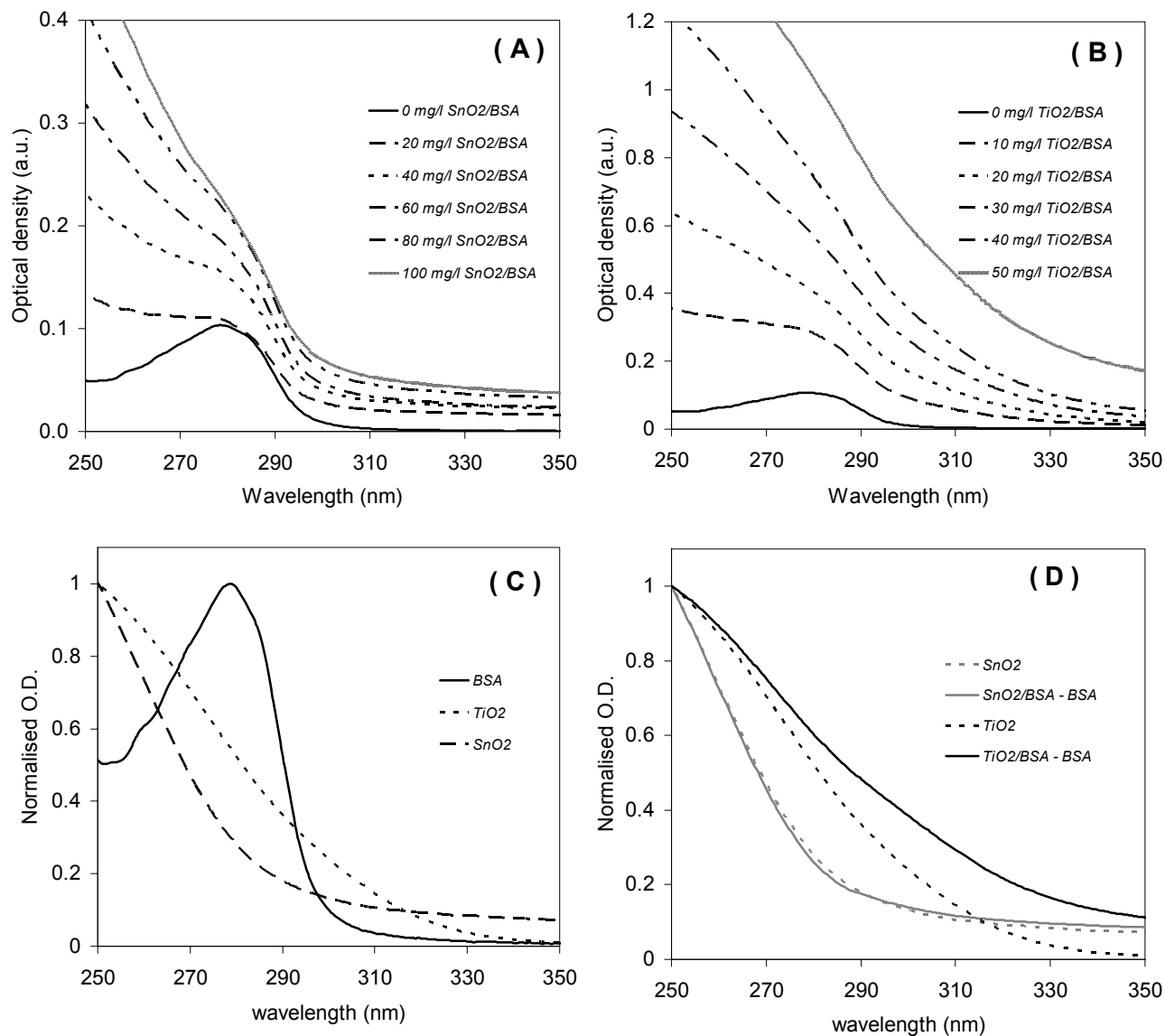


Fig. 2. UV absorption spectra of BSA with SnO₂ (A), and TiO₂ (B) nanoparticles at different concentrations. The Nanoparticle normalised UV spectra at 250 nm is displayed with normalised BSA UV spectrum in (C). The normalised mathematical subtracted spectra for BSA/SnO₂ and BSA/TiO₂ mixture by BSA spectrum is displayed with normalised 50 mg/l TiO₂ and 100 mg/l SnO₂ NP's (D).

At the highest NP concentration, no fluorescence signals are observed when the NP's are excited at 295 nm. In Fig. 3, the typical fluorescence spectra of the BSA protein are shown. The emission band of the Trp residues in BSA, at around 345 nm, does not shift with the increase of nanoparticle concentration. However, the decrease of fluorescence intensity is observed in solutions of both nanoparticles, indicating some form of quenching process. Comparing SnO₂, and TiO₂ nanoparticles, it is observed that a greater reduction of intensity is seen for TiO₂ NP (fig 3B). This may indicate that BSA interacts differently with TiO₂ than with SnO₂ nanoparticles. N-acetyl-DL-Tryptophan (NAT) fluorescence quenching by the nanoparticles was also studied to compare with BSA fluorescence quenching results.

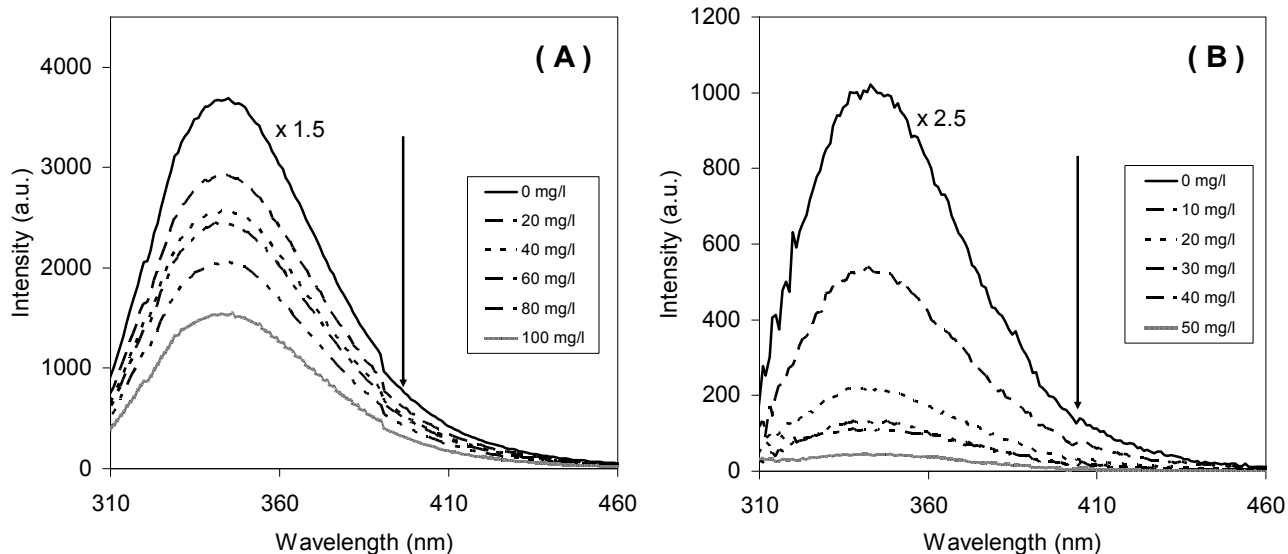


Fig. 3. Fluorescence spectra of BSA with SnO₂ (A), and TiO₂ (B) nanoparticles at different concentrations.

3.3 Fluorescence Lifetimes:

The fluorescence lifetimes of BSA in the presence of nanoparticles were measured using the tryptophan aminoacid residues in the protein structure which have an emission maximum of ~345 nm. The fluorescence decays of BSA were fitted by two exponential with $\tau_1 = 6.8$ ns and $\tau_2 = 3.5$ ns. The first component is responsible for around 70% of the total intensity decay. Using the follow expression, the intensity averaged lifetime can be calculated.

$$\tau_{av} = \frac{\sum a_i \tau_i^2}{\sum a_i \tau_i} \quad (2)$$

where a_i is the pre-exponential factor for a component with lifetime τ_i . Then, the average lifetime calculated for BSA is 6.3 ns. NAT also shows a biexponential decay with $\tau_1 = 4.8$ ns (96.8%) and $\tau_2 = 1.8$ ns (3.2%), and average lifetime of 4.7 ns. This value is close to the 4.5 ns average lifetime found at pH=8.5.¹⁰ In contrast to steady state measurements, the presence of SnO₂ nanoparticles did not affect the fluorescence lifetime of BSA. This is an indication that there is a static quenching contribution to the quenching process of BSA by SnO₂ NP, and similar results were observed for NAT. In contrast to steady state results, neither nanoparticle species were able to quench the fluorescence decay of NAT at the nanosecond time scale of the experiments. This also indicates that NAT quenching process is mainly static. On the other hand, when BSA is excited in the presence of TiO₂ nanoparticles, the average lifetime is reduced reaching a value of 5.9 ns with the increase of TiO₂ NP concentration (Fig 4).

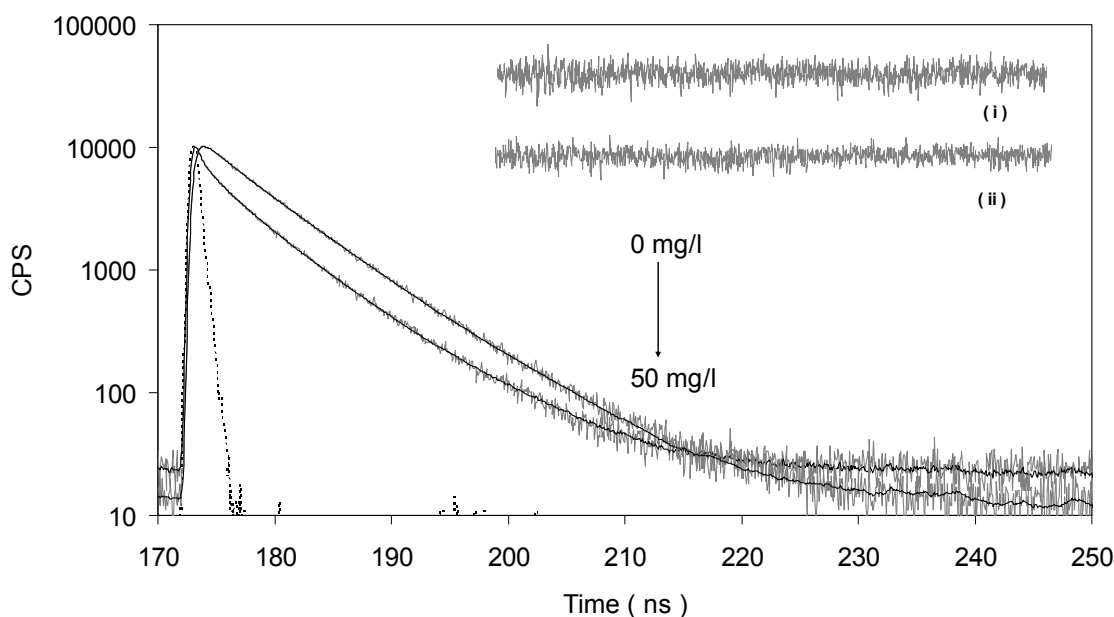


Fig.4. Time resolved fluorescence decay of 2.5 μM BSA at different concentrations of TiO_2 nanoparticle. (Grey lines), biexponential fit (dark lines), and the instrument response function (dotted line). The inset figure shows the residues from the fit. Data collected at 295 nm excitation with the emission measured at 340 nm and a channel resolution of 70 ps.

3.4 Fluorescence Quenching:

Quenching of fluorescence is a decrease in the fluorescence intensity and can be caused by a variety of mechanisms.⁶ Quenching can occur due to non-molecular mechanisms, e.g. attenuation of the incident light by the fluorophore itself or by other absorbing species. Other mechanisms of quenching include a variety of competing processes which induce non-radiative relaxation of excited electrons to the ground state without light emission. These processes can be intramolecular or intermolecular. Intramolecular quenching can occur if a quencher group interacts with the tryptophan aminoacid residue within a distance around 6-10Å.¹¹ The intermolecular quenching processes can be either dynamic and/or static in nature, both of which require some form of molecular contact between the fluorophore and quencher. For this reason, quenching studies can be used as a means of investigation, e.g. to reveal accessibility of fluorophores to quenchers. Dynamic (or collisional) quenching is the deactivation of a fluorophore in the excited state upon contact or collision with another non-fluorescent molecule (quencher) in solution. The fluorophore returns to the ground state due to a diffusional encounter with the quencher; however, the molecules do not undergo chemical modification in the process. The decrease in fluorescence intensity caused by collisional quenching can be described by the Stern–Volmer equation (Eq.3), and the relationship between this decrease in intensity and the quencher concentration is linear:

$$I_0/I = 1 + K_{SV}[Q] \quad (3)$$

where $K_{SV} = k_q \times \tau_0$. k_q is the bimolecular quenching constant, τ_0 is the unquenched fluorescence lifetime, and $[Q]$ is the quencher concentration. Static quenching can occur where the fluorophore and quencher form non-fluorescent complexes or they are within a distance where the quenching occurs during the excitation. The first case occurs in the ground state when the fluorescent species and the quencher molecule form a non-fluorescent complex with an equilibrium constant K_C , and does not depend on diffusion or molecular collisions. The complex limits absorption by reducing the number of active, excitable molecules. Static quenching can be a valuable source of information on binding between a fluorescent sample and a quencher. In the case of static quenching, there is also a linear relationship between

the decrease in fluorescence intensity (I_0/I) and quencher concentration. Equation 4 shows the dependence of fluorescence intensity with quenching concentration when dynamic and static contributions are present.

$$I_0/I = (1 + K_{SV}[Q]) \times (1 + K_C[Q]) \tag{4}$$

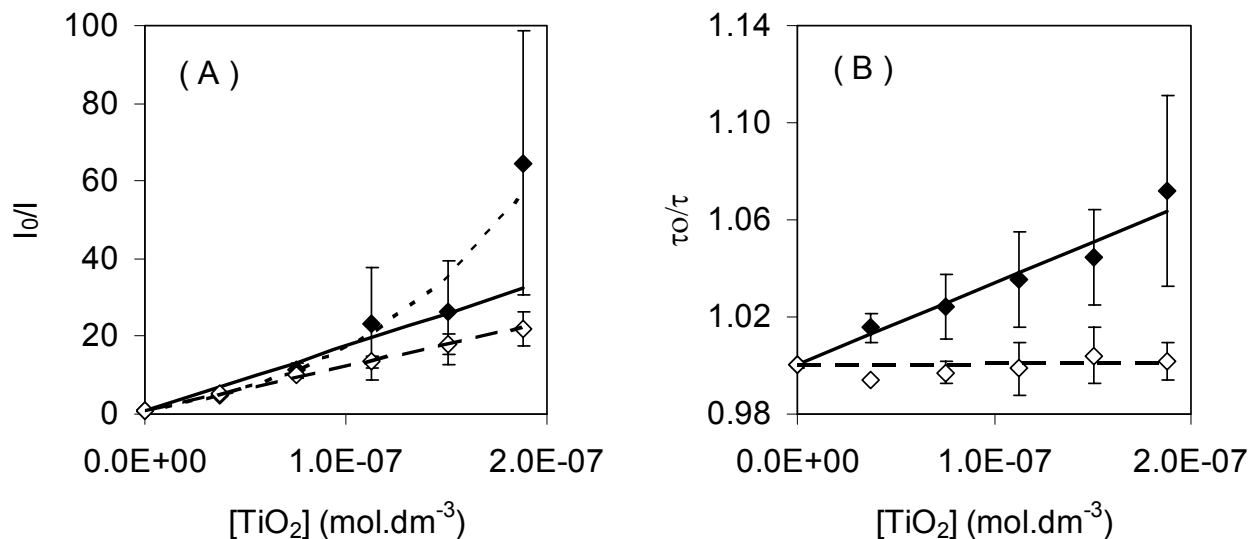


Fig.5. Stern-Volmer plots I_0/I (Panel A) and τ_0/τ (Panel B) against TiO_2 nanoparticle concentration. The filled symbols represent BSA, while NAT quenching data are represented by open symbols. The dark lines are the best fits for BSA fluorescence quenching and dashed line are the best fit for NAT fluorescence quenching. The dotted line in Panel A is the best curve fit data for BSA fluorescence quenching using the sphere of action term (see text).

A second type of static quenching is also possible, this is known as quenching sphere of action (Perrin model).⁶ In this quenching process, the diffusion of both fluorophore and quencher molecules are spatially constrained, during the excitation time scale, in what is termed the quenching sphere of action (QSA) with a molar volume V_m . Therefore, if some of quencher molecules are inside the QSA with the fluorophore at the centre, the fluorescence is assumed to be totally suppressed. On the other hand, there is no perturbation of fluorophore fluorescence if quencher molecule is outside the quenching sphere of action. In the case of the presence of static quenching, the overall quenching process is represented by the most general expression that is the product of equation 4 by the term $\exp(V_m [Q])$, or as expressed by equation 5.

$$I_0/I = (1 + K_{SV}[Q]) \times (1 + K_C[Q]) \times \exp(V_m [Q]) \tag{5}$$

System	$K_{SV}(10^5 M^{-1})$	$K_C (10^5 M^{-1})$
TiO ₂ -NAT	0	1130
TiO ₂ -BSA	3.38 (3.35)*	1580 (707)*
SnO ₂ -NAT	0	3.6
SnO ₂ -BSA	0	4.6

Table. 1. Quenching parameters for Stern-Volmer plots using equation. 4. (*) From equation 5.

The static quenching in combination with dynamic quenching is responsible by the upward curvature in the Stern-Volmer plot (I_0/I) vs. $[Q]$. The lack of any curvature is a sign that one type of quenching is not involved in the mechanism. The steady state fluorescence quenching involves the total process (dynamic and/or static). However, in the time resolved fluorescence quenching only the dynamic quenching is measured. Therefore, lifetime measurements are the most authoritative method of distinguishing between dynamic and static quenching.⁶ As can be seen from Fig. 5, a combination of static and dynamic quenching occurs in BSA/TiO₂ NP case. On the other hand, only static contribution is observed in NAT fluorescence quenching (Fig 5A). Similar results are obtained for BSA and NAT fluorescence quenching by SnO₂ (Fig 6). The quenching parameters using equation 4 are determined by the data fitting and the results displayed in table 1.

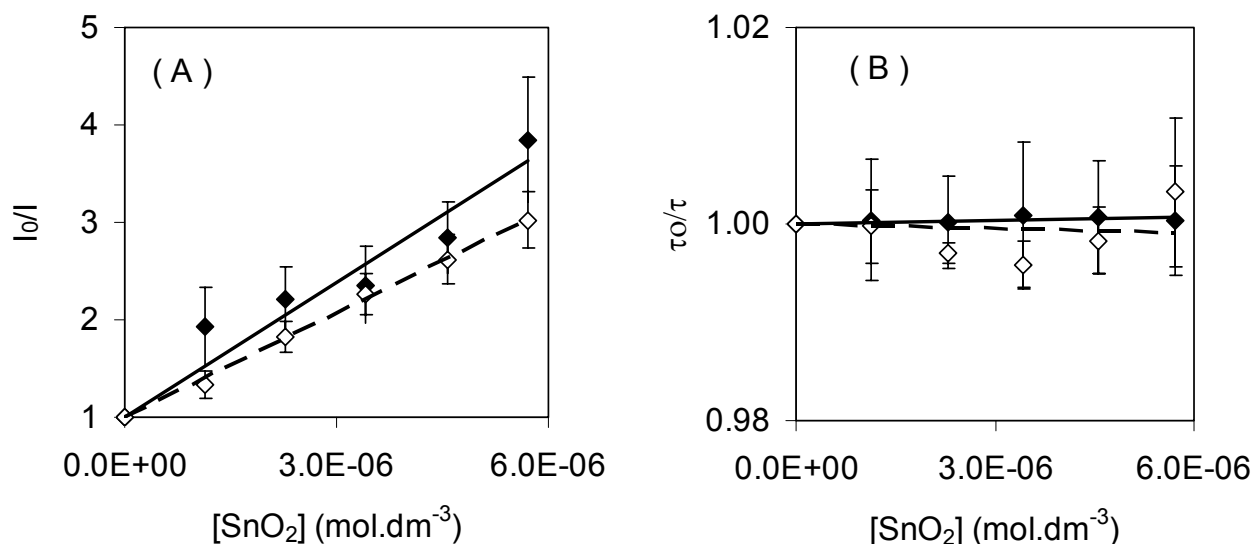


Fig.6. Stern-Volmer plots I_0/I (Panel A) and τ_0/τ (Panel B) against SnO₂ nanoparticle concentration. The solid symbols represent the quenching data of BSA, while NAT quenching data are represented by open symbols. The solid lines are the best curve fit for BSA fluorescence quenching using eq.4 and the dashed line for NAT fluorescence quenching using eq 4.

Although, the contribution of the dynamic process is quite small, relative to the static contribution, the fluorescence quenching of BSA by TiO₂ NP is the only case where the dynamic quenching is consistent (Fig 5B). Taking into account the average fluorescence lifetime of BSA ($\tau_0 = 6.3$ ns), the bimolecular rate constant of dynamic quenching can be calculated by using the K_{SV} ($= kq \times \tau_0$) value in table 1. Therefore, $kq = 5.5 \times 10^{13} M^{-1}s^{-1}$. This value is higher than the estimated diffusion collision rate constant between the fluorophore and quencher molecule in water solution ($\sim 10^{10} M^{-1}s^{-1}$).⁶ Values for bimolecular rate constant greater than diffusion rate constant were found also for the serum albumin protein fluorescence quenching by colloidal gold nanoparticles which suggests a complex formation.¹²

The complex equilibrium constants obtained from the fit indicate that there is a stronger interaction between the protein with TiO₂ nanoparticle than with SnO₂. But, it is important to note that these K_C values are dependent on the particle size used to calculate the concentration, and as mentioned above, TiO₂ nanoparticle size determination was based on conditions different used to those for SnO₂ size determination.

The data in figure 5A can be better fitted (dotted line) if sphere of action static quenching is taken into account (using eq. 5). However, the addition of an extra parameter (V_m) in the model does not change the magnitude of the parameters in table 1. Moreover, the molar volume obtained from the fit of eq. 5 ($V_m \sim 7 \times 10^9 m^{-1}$) represents a sphere of action of approximately 2.8 μm diameter ($V_m = V_o \times N_a$, where V_o is the sphere of action volume and N_a the Avogadro's number), which is around 500 fold larger than the nanoparticle size. This would be possible if the nanoparticles start to aggregate and flocculate in the presence of protein. In fact, as mentioned in the experiment section, TiO₂ NP could not be prepared

in the presence of any electrolyte (buffer salt solution) that became unstable. Also, as mentioned above, the presence of BSA increases the optical density at long wavelengths in the absorption spectra of TiO₂ NP.

Differences in the fluorescence quenching of BSA by NP's and NAT by NP's are small which can mean that the tryptophan aminoacid residues in the protein, are arranged as close as NAT to the NP surface for the respective quenching mechanism. The solubility of TiO₂ and SnO₂ nanoparticles in water is mainly due to an organic layer of trifluoroacetic (TFAc) and acetic (Ac) acids, respectively, bound to the nanoparticle surface.⁷ Due to the fact that the quenching effect on BSA and NAT fluorescence was much stronger with TiO₂ NPs than with SnO₂ NPs in aqueous solution, the TFAc group present on the TiO₂ NPs may be considered as a potential cause of the strong and specific interaction of BSA and NAT with TiO₂ NPs. It has been reported that trifluoroacetic acid binds strongly to BSA¹³. Similar compounds such as halothane (a trifluorocarbon compound) have also high affinity in two binding sites where the two tryptophan aminoacid residues are located in BSA structure¹⁴. TFAc is also described as a strong hydrogen bond donor¹⁵, and does not affect tryptophan or tryptophan derivatives fluorescence¹⁶. Therefore, it is possible that the trifluoroacetic group by hydrogen bonding and/or electrostatic interaction on the TiO₂ NP may enhance the association with BSA and consequently leading to the formation of a non fluorescent complex.

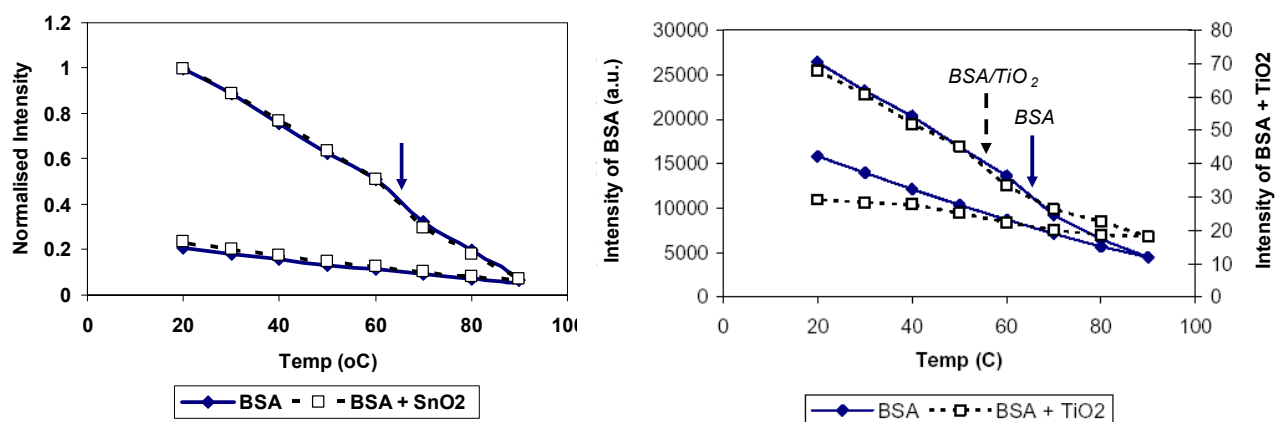


Fig.7: Temperature effect on BSA fluorescence intensity with and without TiO₂ and SnO₂ nanoparticles. The arrows indicate an inflexion point.

The thermal stability of BSA, measured using fluorescence spectroscopy to observe the thermal unfolding of protein was also used to probe the protein-NP interaction.¹⁷ In figure 7, the intrinsic BSA fluorescence intensity was followed by increase-decrease cycle of the temperature (from 20°C to 90°C and then back to 20°C). From analysing the first part of the curves (temperature increase) it is possible to observe a type of sigmoidal unfolding trend as a function of temperature. A small inflexion was noted at a temperature of approximately 65 °C, which is close to the unfolding mid point of ($T_m = 62.1^\circ\text{C}$) found for human serum albumin.¹⁷ It can be seen that in the presence of SnO₂ NP, the BSA fluorescence intensity trend curve with temperature does not change. On the other hand, the presence of TiO₂ nanoparticles modifies the thermal behaviour of BSA fluorescence. In the TiO₂ NP - BSA mixture, the inflexion point of the thermal curve seems to occur at lower temperature (~ 55 °C). The decrease in value for the mid point of unfolding temperature for BSA in the presence of TiO₂ nanoparticles may indicate an interaction, such as hydrogen bonding and/or electrostatic interaction, which can weaken the tertiary protein structure. Consequently, less energy is needed to unfold the protein.

4. CONCLUSIONS

In this work, the interaction of Bovine Serum Albumin (BSA) and two types of soluble metal oxide nanoparticles (titanium and tin) have been studied using the intrinsic fluorescence of tryptophan residue from the proteins measured by steady state and time resolved fluorescence techniques. The Stern-Volmer plots show that quenching process of BSA fluorescence is mainly static by formation of a non fluorescent complex with both metal oxide nanoparticle species. The complex association constant were determined and indicated that BSA interaction with TiO₂ NP is stronger than the interaction with SnO₂ NP. The stability of BSA is also reduced if TiO₂ NP's are present. No spectral shifts in the UV

absorption and fluorescence emission spectra were observed for NPs in solution with BSA, this may indicate that an interaction have to occur in a domain away of tryptophan residues, located at domains I and II, and at same time close to be statically quenched. In other words, BSA may interact with TiO₂ NP through domain III, which is also the most positive charged region of BSA.

5. ACKNOWLEDGEMENTS

The author thanks Dr. P. Fournet for SnO₂ TEM image, and R. Mulryan and D. O'Shaughnessy for the temperature measurements. This work was supported by Science Foundation Ireland under Grant number (02/IN.1/M231), and by an equipment grant from Ireland's Health Research Board (Grant EQ/2004/29).

REFERENCES

1. C.-C.You, M. De, V.M. Rotello, "Monolayer-protected nanoparticle protein interactions." *Curr. Opin. Chem. Biol.* 9, 639-646 (2005).
2. J. Wang, M.L. Clarke, X. Chen, M.A. Even, W.C. Johnson, Z. Chen, "Molecular studies on protein conformations at polymer/liquid interfaces using sum frequency generation vibrational spectroscopy", *Surf. Sci.*, 587, 1-11 (2005).
3. R.A. Latour, "Biomaterials: protein surface interactions." *Encyclopedia of Biomaterial Biomedical Engineering*, Marcel Dekker, New York, pp. 1-15.(2005).
4. O.B. Ptitsyn, A determinable but unresolved problem, *FASEB J*, 10(1), 3-4, (1996) [for more detail see other articles in this special issue of FASEB J].
5. T. Peters Jr., "All About Albumin. Biochemistry, Genetics, and Medical Applications." San Diego, CA: Academic Press (1996).
6. J.R. Lakowicz, "Principles of Fluorescence Spectroscopy." Kluwer Academic/Plenum Press, 2nd ed, NY (1999).
7. The preparation and further details are protected by patent no. WO2005049520.
8. M.J. O'Neil, A. Smith, P.E. Heckelman, S. Budavari, "The Merck index : an encyclopaedia of chemicals, drugs, and biologicals." Merck Publications; 13th edition, Whitehouse Station, N.J. (2001).
9. D. Mc Mahon, D.M. Togashi, A.G. Ryder, unpublished results.
10. S.M. Andrade, S.M.B. Costa, "The Location of Tryptophan, N-acetyltryptophan and a-Chymotrypsin in Reverse Micelles of AOT: A Fluorescence Study" *Photochem. Photobiol.* 72(4), 444-450 (2000).
11. A.G. Szabo, "Fluorescence principles and measurement." M. G. Gore (Ed.). *Spectrophotometry & Spectrofluorimetry*, New York: Oxford, University Press (2000).
12. D. Gao, Y. Tian, S. Bi, Y. Chen, A. Yu, H. Zhang, "Studies on the interaction of colloidal gold and serum albumins by spectral methods." *Spectrochim. Acta Part A*, 62, 1203-1208 (2005).
13. E. Suarez, L. Aguilera, R. Calvo, J.M. Rodriguez-Sasiain, R. Martinez-Jorda, "Effect of halothane anesthesia and trifluoroacetic acid on protein binding of benzodiazepines." *Meth Find Exp Clin Pharmacol*, 13(10), 693-696 (1991).
14. R.G. Eckenhoff, "Aminoacid resolution of Halothane binding sites in serum albumin." *J. Biol. Chem.* 271(26), 15521-6 (1996).
15. K. Sebök-Nagy, L. Biczók, "Effect of protonation and hydrogen bonding on the fluorescent properties and exciplex formation of N-(4-pyridyl)-1,2-naphthalimide." *Photochem. Photobiol. Sci.* 3, 389-395 (2004).
16. P. Midoux, P. Wahl, J.-C Aucht, M. Monsigny, "Fluorescence quenching of tryptophan by trifluoroacetamide." *Biochim. Biophys. Acta*, 801, 16-25 (1984).
17. G.A. Pico, "Thermodynamic feature of the thermal unfolding of human serum albumin." *Int. J. Biol. Macromol.* 20, 63-73 (1997).